Auger neutralization rate for slow Ar+ ions in front of KCl(001)

AUTHOR(S):

Kimura, K; Tsujioka, T; Tanaka, S; Nakamoto, A; Nakajima, K; Suzuki, M

CITATION:

Kimura, K ...[et al]. Auger neutralization rate for slow Ar+ ions in front of KCl(001). PHYSICAL REVIEW A 2004, 70(2): 022901.

ISSUE DATE:

2004-08

URL:

http://hdl.handle.net/2433/39827

PHYSICAL REVIEW A **70**, 022901 (2004)

Auger neutralization rate for slow Ar^+ ions in front of KCl(001)

K. Kimura,* T. Tsujioka, S. Tanaka, A. Nakamoto, K. Nakajima, and M. Suzuki
Department of Engineering Physics and Mechanics, Kyoto University, Kyoto 606-8501, Japan
(Received 14 August 2003; published 31 August 2004)

Angular and charge-state distributions are measured for 5–15-keV. Ar^0 and Ar^+ ions reflected from a KCl(001) surface under glazing angle incidence. The ionization of Ar^0 is almost completely suppressed at incident angles smaller than a critical angle (11–22 mrad, depending on the ion energy), while a considerable fraction of incident Ar^+ ions are neutralized. It is demonstrated that a position-dependent Auger neutralization rate can be derived from the observed result without any assumption except for the surface continuum potential. The obtained Auger neutralization rate shows a simple exponential dependence as is usually assumed.

DOI: 10.1103/PhysRevA.70.022901 PACS number(s): 79.20.Rf, 61.85.+p, 79.60.Bm

I. INTRODUCTION

Since the pioneering work by Hagstrum [1], charge exchange phenomena between ions and solid surfaces have been studied extensively for several decades. In a low-energy regime, there are two dominant charge exchange mechanisms: one is a resonant one-electron tunneling process and the other is a two-electron Auger process. In general, Auger neutralization plays an important role for the neutralization of noble gas ions [2].

When an ion is scattered by a surface atom, the survival probability from the Auger neutralization process is given by

$$F^+ = e^{-v_c(1/v_{i\perp}+1/v_{f\perp})}, \tag{1}$$

where $v_{i\perp}$ and $v_{f\perp}$ denote perpendicular components of initial and final ion velocities, respectively, and the so-called characteristic velocity v_c is defined by integration of the Auger transition rate $P(x)$ from 0 to ∞—i.e., $v_c=\int_0^\infty P(x)dx$, where x is the distance from the surface. The charge exchange processes in the violent single collisions with surface atoms are neglected in Eq. (1), and this is actually the case when the ion energy is less than a threshold energy E_{th} (e.g., $E_{th}\sim 2$ keV for He^+ scattered by 129° from a Cu surface) [3]. Thus, by measuring F^+ as a function of $v_{i\perp}$ and/or $v_{f\perp}$ the characteristic velocity v_c for the Auger neutralization can be easily determined. However, the Auger neutralization rate $P(x)$ itself is difficult to be deduced from the charge distribution measurement.

Recently, Hecht *et al.* have shown that the Auger transition rate of 2-keV He^+ ions in front of an Al surface can be derived from a detailed analysis of image charge effects on the trajectories of ions scattered at grazing angle incidence [4]. Their method is based on the fact that He^+ ion is accelerated toward the surface by the image potential but He^0 is not [5]. As a result, the scattering angle depends on where the incident He^+ ion is neutralized. Thus, the information of the Auger neutralization rate can be obtained from the observed angular distributions of the scattered He^0 and He^+ ions. They assumed a simple formula—i.e., $P(x)=P_0\exp(-x/a)$—for the Auger neutralization rate as was first introduced by Hagstrum. They calculated the angular distributions of He^0 and He^+ ions scattered from Al(111) by means of a Monte Carlo simulation. The preexponential factor P_0 and the decay length a were determined by comparing the calculated result with the observed one. However, as was pointed out by More *et al.*, the angular distribution is very sensitive with respect to the representation of the image potential [6], indicating that accurate derivation of $P(x)$ is rather difficult. Moreover, recent theoretical studies showed that the Auger neutralization rate deviates from the simple exponential decay [7–9].

In this paper, we propose a method to derive the position-dependent Auger neutralization rate from the charge-state distribution measurement. This approach is straight-forward and no parameter fitting procedure is required. An example of the analysis is performed for 5–15-keV Ar^+ ions on KCl(001). In this system, resonant neutralization and ionization are not allowed and only Auger neutralization can take place with help of a Doppler-shifted Cl $3p$ band and/or surface states [2,10].

II. EXPERIMENT

A single crystal of KCl was cleaved along (001) plane in air and was mounted on a five-axis precision goniometer in an UHV chamber (base pressure 2×10^{-10} Torr). The surface was heated at 300 °C to prepare a clean surface [11] and kept at 250 °C to avoid surface charging during the measurement [12]. A beam of 5–15-keV Ar^+ ions from a 10-GHz ECR ion source was collimated to 0.1×0.1 mm^2 by a series of apertures and was incident to the KCl(001) surface at a grazing angle θ_i with respect to the surface plane. The energy dispersion in the incident beam was less than 0.3%. The reflected Ar ions were resolved into their charge states by means of electric field plates and detected by a two-dimensional position-sensitive detector (2D-PSD) placed 160 mm downstream of the target. The 2D-PSD consisted of Z-stack microchannel plates (MCP's) and a resistive anode (effective diameter 40 mm). The signals from the resistive anode were converted to digital signals and were stored in list mode. Because the gain of the MCP's was not uniform, the discrimination level for noise elimination was changed

*Author to whom correspondence should be addressed. FAX: +81-75-753-5253. Electronic address: kimura@kues.kyoto-u.ac.jp

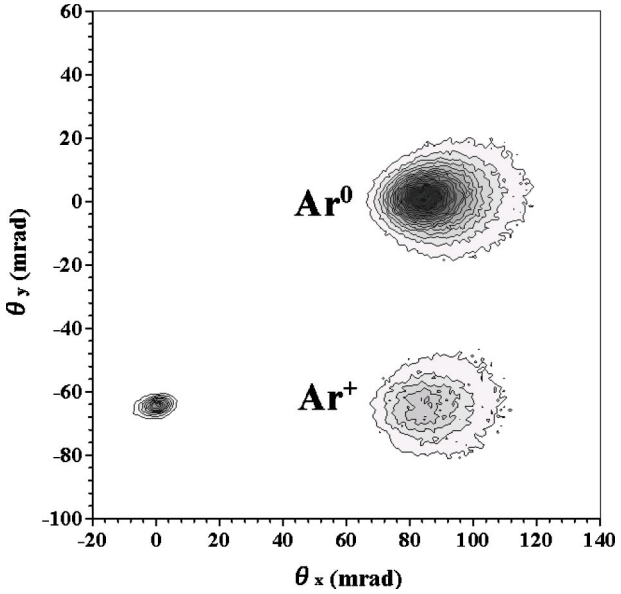

FIG. 1. Angular distribution of scattered Ar ions measured by 2D-PSD when 10-keV Ar^+ ions are incident on a KCl(001) surface at $\theta_i = 42$ mrad. The large (small) broad peak correspond to $Ar^0(Ar^+)$. The sharp peak represents the residual incident beam.

from position to position depending on the local gain of the MCP's. It should be noted that the efficiency of the MCP's does not depend on the charge state of the ion and is primarily determined by the ion energy if the noise discrimination level is carefully chosen [13].

For the experiment of Ar^0 incidence, the vacuum of the beam line was changed from 10^{-8} Torr to 10^{-7} Torr. Neutral Ar atoms produced by charge exchange collisions with residual gas molecules were selected by a magnetic deflector installed just before the scattering chamber and the obtained Ar^0 beam was used as an incident beam.

III. RESULTS

Figure 1 shows an example of observed angular distribution of reflected ions when 10 keV Ar^+ ions were incident on KCl(001) at $\theta_i = 42$ mrad. There are three well-defined peaks. The sharp peak represents the residual incident beam. The full width at half maximum (FWHM) of the incident beam is about 6 mrad, which gives the overall angular resolution of the present system including the angular spread of the incident beam. The broad peaks correspond to the reflected Ar^0 atoms (large peak) and Ar^+ ions (small peak), which were resolved by the electric field plates. There was no Ar ion other than Ar^0 and Ar^+. The observed peaks were able to be fitted to Gaussian functions resonably well. The mean scattering angles for Ar^0 and Ar^+ were derived from the observed angular distribution.

Figure 2 shows the scattering angle as a function of θ_i for 10 keV Ar^+ incidence. Although the scattering angle for Ar^+ agrees with the specular angle, the behavior of Ar^0 is slightly complicated. At small θ_i (<25 mrad) the scattering angle for Ar^0 is larger than the specular angle due to the image acceleration [5]. At larger θ_i, however, the scattering angle for Ar^0

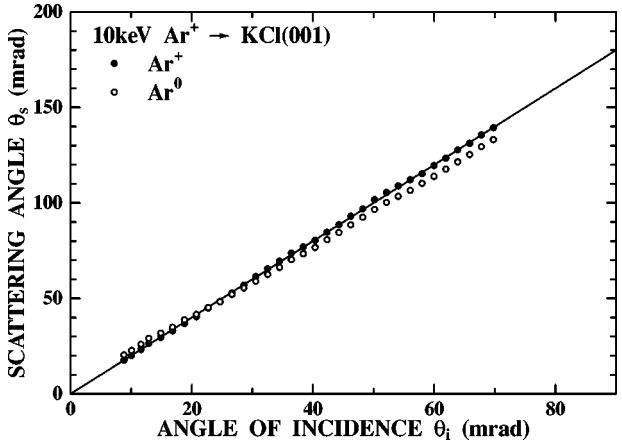

FIG. 2. The angle of scattering for Ar^+ (solid circles) and Ar^0 (open circles) as a function of the angle of incidence. The incident ion is 10 keV Ar^+.

is smaller than the specular angle, suggesting that Ar^+ is decelerated upon electron capture at larger θ_i. Similar results were obtained for 5 and 15 keV Ar^+ incidence.

The neutral fraction of the reflected Ar beam can be obtained from the observed angular distribution. Figure 3 shows the observed Ar^0 fraction F^0 as a function of θ_i. The solid symbols show the results for Ar^+ incidence and the open symbols show the results for Ar^0 incidence. The observed neutral fraction does not depend on the incident charge states at large θ_i, indicating that the memory of the incident charge state is lost and a kind of charge state equilibrium is achieved. On the other hand, the ionization of Ar^0 is almost completely suppressed at small θ_i, indicating that there is a critical incident angle for ionization process. The critical incident angle for ionization was estimated to be about 22, 16, and 11 mrad for 5, 10, and 15 keV Ar^0 as is shown in Fig. 3. The distance of the closest approach corresponding to the critical angle is almost independent of the ion energy and is estimated to be 3.7 ± 0.2 a.u., where the

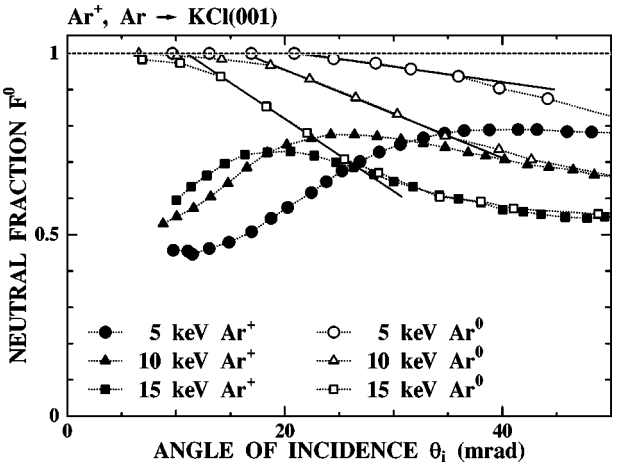

FIG. 3. Observed Ar^0 fraction as a function of angle of incidence for 5–15 keV Ar^+ and Ar^0 scattered from KCl(001). At small θ_i ionization of Ar^0 is almost completely suppressed while the neutralization of Ar^+ takes place.

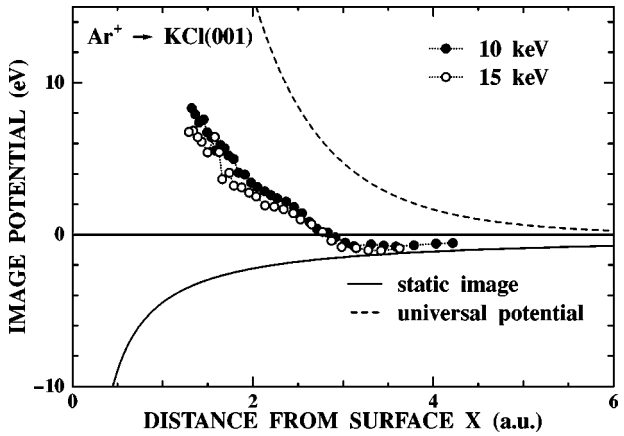

FIG. 4. Image potential estimated from the observed scattering angles for Ar^+ and Ar^0. The results obtained from the data of 10 keV Ar^+ incidence (solid circles) and 15 keV Ar^+ incidence (open circles) are shown. The static image potential is shown by a solid curve. The obtained image potential is about two-thirds of the static image at x larger than ~3.5 a.u.

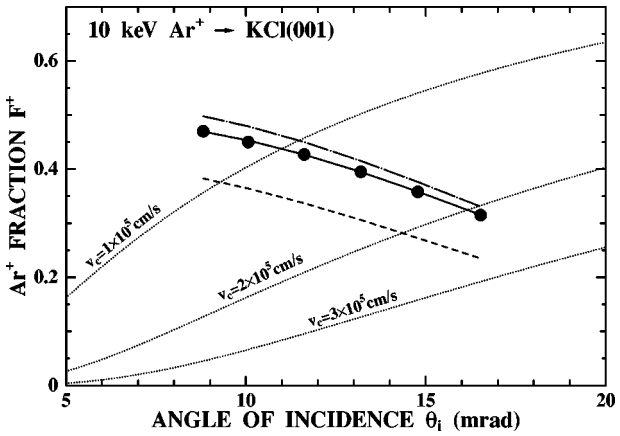

FIG. 5. Observed Ar^+ fraction as a function of angle of incidence for 10 keV Ar^+ scattered from KCl(001). The dotted curves show the ion fraction calculated with Eq. (1) for various v_c.

universal potential [16] was enployed for ion-surface interaction potential. On the other hand, the incident Ar^+ ions have a large chance to capture electrons even at θ_i smaller than the critical angle.

The observed suppression of ionization is in harmony with the fact that the resonant ionization of Ar^0 is not allowed in front of KCl surface because of its wide band gap. Thus the observed results can be analyzed without the reionization process when θ_i is smaller than the critical angle. This allows us to derive the position-dependent neutralization rate $P(x)$ from the observed result as will be shown in the next section.

IV. DISCUSSION

When the incident Ar^+ ion capture an electron in front of KCl(001) surface the Ar ion gets an energy corresponding to the image potential. The energy gain can be estimated from the observed scattering angle

$$\Delta E_g = E\{\sin^2(\theta_s^n - \theta_i) - \sin^2\theta_i\}, \tag{2}$$

where E is the ion enrgy and θ_s^n denotes the scattering angle of Ar^0 for Ar^+ incidence. Because the neutralization occurs mainly around the turning point of the ion trajectory, the obtained energy gain represents the image potential at the turning point. The position of the turning point, x_{min}, can be calculated by $E\sin^2(\theta_s^n - \theta_i) = V_0(x_{min})$, where $V_0(x)$ is the surface continuum potential for Ar^0. Thus we can derive the image potential as a function of x from the observed scattering angles. Figure 4 shows the obtained image potential as a function of x. In the calculation, we employed the universal potential for $V_0(x)$. The solid curve shows the static image potential $\{[1-\epsilon(0)]/[1+\epsilon(0)]\}e^2/4x$, where $\epsilon(0)$ is a static dielectric constant [$\epsilon(0)=4.85$ for KCl].

The present result indicates that the image potential roughly follows the static image at x larger than ~3.5 a.u. but the magnitude of the image potential is about two-thirds of the classical image. The reduction of image potential can be attributed to the dynamical aspect of the image potential [14]. The high-frequency limit of the dielectric constant is $\epsilon(\infty)=2.1$ for KCl. The dynamical image potential should be somewhere in between $\{[1-\epsilon(0)]/[1+\epsilon(0)]\}e^2/4x$ and $\{[1-\epsilon(\infty)]/[1+\epsilon(\infty)]\}e^2/4x$.

With decreasing x the observed image potential deviates from the static image considerably and becomes even positive. The deviation can be ascribed to the energy level shift of Ar^0 in front of KCl(001) surface. Precisely speaking, the observed energy gain is not the image potential itself but the difference between Ar^+-KCl(001) and Ar^0-KCl(001) interaction potentials. Recently More *et al.* discussed the effect of the energy level shift on the energy gain upon neutralization of He^+ in front of Al(001) [6]. They calculated the total energy for He-Al(001) system and showed that the energy gain deviates from the image potential at x smaller than ~5 a.u. Our present result qualitatively agrees with their theoretical result.

Figure 5 shows comparison between the observed ion fraction F^+ and the result of simple calculation for 10 keV Ar^+ incidence. The dotted curves show the ion fraction calculated with Eq. (1) for various v_c, where the incoming and outgoing trajectories of the ion were assumed to be straight lines. The θ_i dependence of the calculated Ar^+ fraction is entirely different from the observed result. This discrepancy indicates that the details of the ion trajectory $x(t)$ should be taken into account to explain the present experimental result. The ion trajectory can be calculated by the equation

$$\frac{dx}{dt} = \sqrt{\frac{2\{V(x_{\min}) - V(x)\}}{M}}, \tag{3}$$

where M is the ion mass, $V(x)$ is the surface continuum potential, and x_{min} is the distance of the closest approach of the ion. Recalling that reionization is almost completely suppressed at $x > 3.7$ a.u., the evolution of F^+ is governed by a simple rate equation

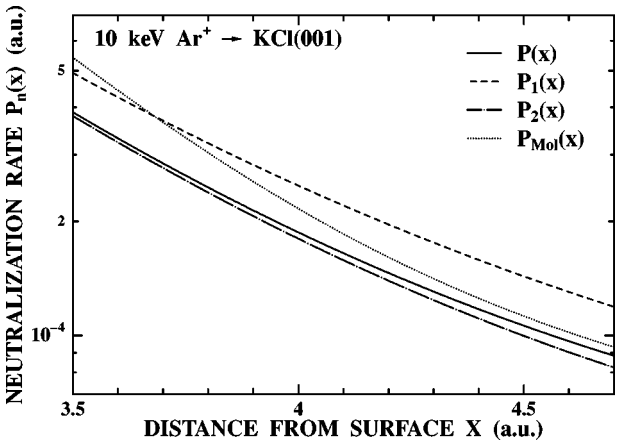

FIG. 6. Auger neutralization rate for 10 keV Ar^+ in front of KCl(001) derived from the observed Ar^+ fraction (the solid curve). The result obtained by neglecting the image force is shown by a dashed curve (see text). The result derived with Molière potential is also shown by a dotted curve.

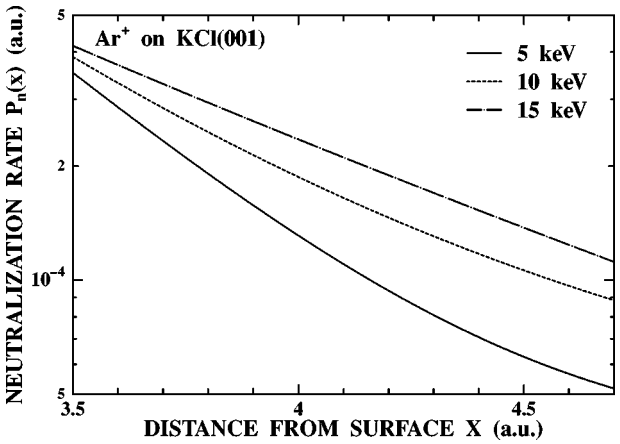

FIG. 7. Auger neutralization rates for 5 keV Ar^+ (solid curve), 10 keV Ar^+ (dashed curve), and 15 keV Ar^+ (dot-dashed curve). The neutralization rate increases with the ion energy.

$$\frac{dF^+(t)}{dt} = -P(x(t))F^+(t), \tag{4}$$

where $P(x)$ is the position-dependent neutralization rate. The solution of the equation is given by

$$F^+(\theta_i) = \exp\left\{-\int_{-\infty}^{+\infty} P(x(t))dt\right\}. \tag{5}$$

Substituting Eq. (3) into Eq. (5), one can find an integral equation of the Abel type:

$$G(\theta_i) = \int_{x_{\min}}^{\infty} \frac{\sqrt{2M}P(x)}{\sqrt{V(x_{\min}) - V(x)}}dx, \tag{6}$$

where $G(\theta_i)$ is defined as $-\ln[F^+(\theta_i)]$. If $V(x)$ is a monotonic function, the solution of Eq. (6) is given by

$$P(x) = -\frac{1}{\pi M v}\frac{dV(x)}{dx}\left\{G(0)\sqrt{\frac{E}{V(x)}} + \int_0^{\pi/2}\frac{dG(\theta_i)}{d\theta_i}\bigg|_{\theta_i=\sqrt{V(x)/E}\,\sin(u)} du\right\}, \tag{7}$$

where v is the ion velocity and E is the ion energy. The energy loss of the projectile ion is neglected because it is less than a few % of the incident energy [15]. This equation means that the position-dependent neutralization rate $P(x)$ can be derived from the observed $F^+(\theta_i)$.

The actual $V(x)$ is not a monotonic function due to the existence of the image potential. Nevertheless, we first neglect the image potential to estimate $P(x)$—i.e., the surface continuum potential $V_0(x)$ excluding the image potential is used in Eq. (7) instead of the total potential $V(x)$. The result of the first approximation, $P_1(x)$, is shown by a dashed curve in Fig. 6. In the calculation, we employed the universal potential [16] for $V_0(x)$. By integrating $P_1(x)$ along the ion trajectory, the Ar^+ fraction, $F_1^+(\theta_i)$, can be obtained with Eq. (5). We used the above-mentioned image potential $\frac{2}{3}\{[1-\epsilon(0)]/[1+\epsilon(0)]\}e^2/4x$ in the calculation of the ion trajectory. The obtained result, shown by a dashed curve in Fig. 5, disagrees with the experimental one, because the image potential was neglected in the derivation of $P_1(x)$. A correction $\Delta P_1(x)$ to $P_1(x)$ can be calculated with Eq. (7) by substituting $\Delta G_1(\theta_i) \equiv \ln[F_1^+(\theta_i)] - \ln[F_{expt}^+(\theta_i)]$ and $V_0(x)$ instead of $G(\theta_i)$ and $V(x)$, respectively. The corrected result $P_2(x) = P_1(x) + \Delta P_1(x)$ is shown by a dot-dashed curve in Fig. 6, which is smaller than $P_1(x)$ by ~30%. The ion fraction $F_2^+(\theta_i)$ calculated with the corrected rate $P_2(x)$ is shown by a dot-dashed curve in Fig. 5. The agreement with the experimental result is improved very much as compared with the first approximation. Repeating these procedures several times, $F_n^+(\theta_i)$ finally converges on the experimental result as shown by a solid curve and the position-dependent Auger neutralization rate is obtained. The resulting Auger neutralization rate is shown by a solid curve in Fig. 6.

The obtained Auger neutralization rate increases almost exponentially with decreasing x as is usually assumed. In the present method, the neutralization rate was derived from the experimental results without any assumption except for the surface continuum potential $V_0(x)$ for which the universal potential was used. Here, the neutralization rate is derived with other realistic potential—i.e., the Molière potential—to see if the choice of the potential is crucial for derivation of $P(x)$ or not. The obtained result is shown by a dotted curve in Fig. 6. The result for the Molière potential is larger than that for the universal potential, but the difference is not so large, indicating that the error caused by the choice of potential is not serious.

Figure 7 shows the Auger neutralization rates for 5, 10, and 15 keV Ar^+. The neutralization rate increases with ion energy. This energy dependence is related with the fact that the Auger neutralization is not allowed in the static limit [2] due to the large band gap of KCl. The Auger neutralization can take place with help of kinematical effect. The observed energy dependence supports this scenario.

Recently, Wethekam *et al.* showed that Auger neutralization rate for keV He^+ ions in front of Ag(111) can be esti-

mated from the observed E dependence of the He^+ fraction after grazing angle scattering [17]. In their method the x dependence of the Auger neutralization rate must be assumed. They used a simple exponential function—i.e., $P(x) = P_0 \exp(-x/a)$. In this respect we point out that our present method requires no assumption about $P(x)$. The only requirement is knowledge of the interaction potential.

V. CONCLUSION

Charge-state distributions and scattering angle distributions of reflected ions have been measured when 5–15-keV Ar^0 and Ar^+ ions were incident on a KCl(001) surface at a grazing angle. It is found that ionization process is almost completely suppressed at x larger than ~3.7 a.u.. The image potential for Ar^+ is estimated from the observed angular distribution. The obtained image potential is about two-thirds of the static image potential at x larger than ~3.5 a.u., while large discrepancy is observed at smaller x. This discrepancy is attributed to the shift of the energy level of Ar^0 in front of the surface. It is demonstrated that the position-dependent Auger neutralization rate can be derived from the observed Ar^+ fraction without any assumption other than the ion-surface interaction potential. The obtained Auger neutralization rate shows a simple exponential decay as is usually assumed. The Auger neutralization rate is found to increase with ion energy, indicating that the Auger neutralization takes place with help of kinematical effect in the present case.

ACKNOWLEDGMENTS

We are grateful to Professor J. Burgdörfer for fruitful discussion. This work was supported in part by the Center of Excellence for Research and Education on Complex Functional Mechanical Systems (COE program) of the Ministry of Education, Culture, Sports, Science and Technology, Japan.

[1] H. D. Hagstrum, Phys. Rev. **96**, 336 (1954).
[2] H. Winter, Phys. Rep. **367**, 387 (2002).
[3] M. Draxler, R. Gruber, H. H. Brongersma, and P. Bauer, Phys. Rev. Lett. **89**, 263201 (2002).
[4] T. Hecht, H. Winter, and A. G. Borisov, Surf. Sci. **406**, L607 (1998).
[5] H. Winter, Europhys. Lett. **18**, 207 (1992).
[6] W. More, J. Merino, R. Monreal, P. Pou, and F. Flores, Phys. Rev. B **58**, 7385 (1998).
[7] H. Jouin, F. A. Gutierrez, and C. Harel, Phys. Rev. A **63**, 052901 (2001).
[8] N. Lorente and R. Monreal, Surf. Sci. **370**, 324 (1997).
[9] M. A. Cazalilla, N. Lorente, R. D. Muino, J.-P. Gauyacq, D. Teillet-Billy, and P. M. Echenique, Phys. Rev. B **58**, 13991 (1998).
[10] T. Hecht, C. Auth, A. G. Borisov, and H. Winter, Phys. Lett. A **220**, 102 (1996).
[11] M. Prutton, *Surface Physics* (Claredon, Oxford, 1983), p. 9.
[12] K. Kimura, G. Andou, and K. Nakajima, Phys. Rev. Lett. **81**, 5438 (1998).
[13] M. Barat, J. C. Brenot, J. A. Fayeton, and Y. J. Picard, Rev. Sci. Instrum. **71**, 2050 (2000).
[14] H. Winter, Prog. Surf. Sci. **63**, 177 (2000).
[15] K. Nakajima, M. Nakamura, T. Tsujioka, and K. Kimura, Nucl. Instrum. Methods Phys. Res. B **205**, 705 (2003).
[16] J. F. Ziegler, J. P. Biersack, and U. Littmark, *The Stopping and Range of Ions in Solids* (Pergamon Press, New York, 1985), Vol. 1.
[17] S. Wethekam, A. Mertens, and H. Winter, Phys. Rev. Lett. **90**, 037602 (2003).